Journal of the Neurological Sciences 408 (2020) 116529

Contents lists available at ScienceDirect

Journal of the Neurological Sciences

journal homepage: www.elsevier.com/locate/jns

Measuring graphical strength within the connectome: A neuroanatomic, parcellation-based study

Ryan G. Jones[a], Robert G. Briggs[b], Andrew K. Conner[a], Phillip A. Bonney[b], Luke R. Fletcher[a], Syed A. Ahsan[c], Arpan R. Chakraborty[a], Cameron E. Nix[a], Christina C. Jacobs[a], Alison M. Lack[a], Daniel T. Griffin[a], Charles Teo[c], Michael E. Sughrue[c,*]

[a] Department of Neurosurgery, University of Oklahoma Health Science Center, Oklahoma City, OK, United States of America
[b] Department of Neurosurgery, University of Southern California Keck School of Medicine, Los Angeles, CA, United States of America
[c] Center for Minimally Invasive Neurosurgery, Prince of Wales Private Hospital, Sydney, Australia

ARTICLE INFO

Keywords:
Edges
Graph theory
Matrix
Neurosurgery
Nodes
Strength
Tractography

ABSTRACT

Introduction: Graph theory is a promising mathematical tool to study the connectome. However, little research has been undertaken to correlate graph metrics to functional properties of the brain. In this study, we report a unique association between the strength of cortical regions and their function.

Methods: Eight structural graphs were constructed within DSI Studio using publicly available imaging data derived from the Human Connectome Project. Whole-brain fiber tractography was performed to quantify the strength of each cortical region comprising our atlas.

Results: Rank-order analysis revealed 27 distinct areas with high average strength, several of which are associated with eloquent cortical functions. Area 4 localizes to the primary motor cortex and is important for fine motor control. Areas 2, 3a and 3b localize to the primary sensory cortex and are involved in primary sensory processing. Areas V1-V4 in the occipital pole are involved in primary visual processing. Several language areas, including area 44, were also found to have high average strength.

Conclusions: Regions of average high strength tend to localize to eloquent areas of the brain, such as the primary sensorimotor cortex, primary visual cortex, and Broca's area. Future studies will examine the dynamic effects of neurologic disease on this metric.

1. Introduction

Graph theory has been widely applied to social and biological systems, including the human brain [1–5]. Using this method of analysis, the brain is divided into discrete cortical regions so the structural or functional connections between them can be measured. In graph theory parlance, the distinct areas of cortex defined in the analysis are called “nodes”, while the structural or functional connections between them are called “edges”. Analyzing these connections typically involves measuring different graph theory metrics. Study of these metrics has led to discoveries critical to our understanding of the human connectome [1,5–8].

Strength is a graph metric that quantifies the total number of structural or functional connections to a single node based on the type of graph under consideration [9]. In structural graphs, strength represents a quantification of the total number of nerve fibers or axons connected to a single node of gray matter. Our understanding of the relevance of graphical strength to neuroanatomy remains poorly understood, as there is a paucity of literature describing the strength of different cortical regions in the neurosurgical literature.

In this study, we generated eight graph matrices using imaging data made available through the Human Connectome Project (HCP). The matrices were constructed based on an atlas of 180 distinct cortical regions in the left cerebral hemisphere [10]. The matrices were weighted by the number of fiber tracts terminating within these distinct regions of interest (ROIs) and were used to measure the strength of each region as defined in our atlas. Average strengths were computed across all eight subjects to better understand which parts of the cortex are associated with high and low strength within the left cerebral hemisphere. The goal of this project was to contextualize node strength within a useful neurosurgical framework.

* Corresponding author at: Suite 3, Level 7 Prince of Wales Private Hospital, Barker Street, Randwick, New South Wales 2031, Australia.
E-mail address: sughruevs@gmail.com (M.E. Sughrue).

https://doi.org/10.1016/j.jns.2019.116529
Received 23 April 2019; Received in revised form 8 October 2019; Accepted 9 October 2019
Available online 01 November 2019
0022-510X/

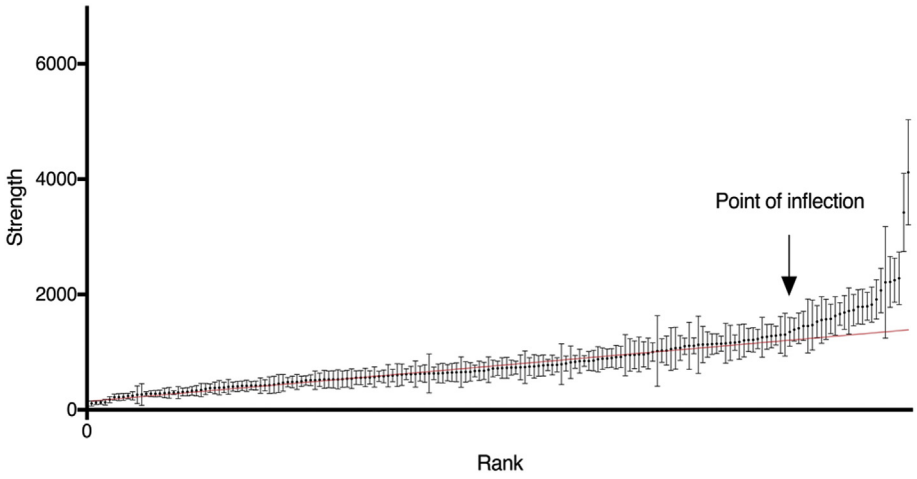

Fig. 1. Ranked distribution of all 180 cortical regions included in our atlas according to their average strength as measured across the eight subjects included in this analysis. Regions are plotted in order of least to greatest strength. Dots signify the mean strength with associated standard error bars. Linear regression was used to generate a line-of-best-fit (in red) for ranks 1–152 (Pearson's $R^2 = 0.988$, $p < .0001$). A point of inflection is discernible at ROI rank 153 (black arrow). (For interpretation of the references to colour in this figure legend, the reader is referred to the web version of this article.)

Table 1
List of cortical regions associated with the highest average strength.

Cortical region	Average strength ± SEM	Cortical region	Average strength ± SEM
V1	4119 ± 911	FOP4	1688 ± 292
V2	3424 ± 680	PI	1661 ± 196
V3	2279 ± 456	V4	1629 ± 333
6r	2248 ± 382	44	1575 ± 259
TGd	2218 ± 442	TE1p	1570 ± 351
PIR	2210 ± 969	FOP3	1559 ± 406
4	2071 ± 386	RSC	1530 ± 279
PFm	1913 ± 343	TE2a	1470 ± 435
PreS	1826 ± 303	PeEc	1456 ± 467
2	1795 ± 243	PGi	1455 ± 253
3b	1789 ± 304	RI	1412 ± 265
3a	1789 ± 296	PH	1390 ± 200
V3A	1727 ± 271	PGs	1350 ± 249
8C	1715 ± 403		

2. Methods

2.1. Obtaining connectome images

Publicly available imaging data was obtained for this study through the HCP database (http://humanconnectome.org, release Q3). Diffusion imaging scans from eight healthy, unrelated subjects were used for fiber tracking analysis (Subjects IDs: 100307, 105115, 111312, 113619, 115320, 117112, 118730, 118932). The diffusion data were reconstructed using generalized q-sampling imaging within DSI Studio (Carnegie Mellon, http://dsi-studio.labsolver.org) with a specified diffusion sampling length ratio of 1.25 [11]. A multi-shell diffusion scheme was used with b-values of 990, 1985, and 1980 s/mm^2. Each b-value was sampled in 90 directions. The in-plane resolution was 1.25 mm.

2.2. Generation of structural matrices and measurement of strength

In order to generate a structural matrix, we first had to select a cortical atlas. We based our atlas on the cortical parcellation scheme previously published under the HCP [12]. All subject brain imaging as well as all regions contained within our atlas were registered to the Montreal Neurologic Institute (MNI) coordinate space [13]. The atlas ROIs were then loaded into DSI Studio and moved into the correct anatomic position based on the supplementary details accompanying the original article parcellating the human cortex [12].

After ensuring each ROI was in its proper anatomic position, whole-brain fiber tractography was performed in DSI Studio (Carnegie Mellon, http://dsi-studio.labsolver.org) [14]. A total of 2.5 million seeds were randomly placed. Voxels were automatically traced with a maximum angular threshold of 45 degrees. Tracks with length shorter than 10 mm or longer than 800 mm were discarded. The cortical atlas consisting of the anatomic ROIs was then loaded onto the relevant subject brain. The number of fiber tracts terminating between regions was used to generate a structural connectivity matrix for each subject. Graph theoretical measures, including strength, were computed in DSI Studio and exported to Microsoft Excel for further quantitative analysis.

2.3. Statistical analysis and rank figure construction

Average nodal strength was measured for each region across all eight subjects included in this analysis. To compare strength between parcellations, we standardized average strength measurements by the ROI volume of each node from the atlas as measured in MNI space. Standardized strength values were ranked from lowest to highest and compared graphically using GraphPad Prism 7 (GraphPad Software, San Diego, California, United States). Linear regression was used to calculate a Pearson Coefficient between strength and rank for all 180 cortical areas of interest in our atlas. The Spearman Correlation Test was performed to assess for a correlation between the volume and strength. Coefficients of variation were also measured to quantify the variation in strength as measured across subjects. Finally, to measure the effects of volume standardization on strength, we charted the absolute value change in rank position for parcellations after standardizing average strength measurements.

3. Results

The distribution of average strength values for all 180 parcellations is shown in Fig. 1. For ROIs of rank 1–152, the line-of-best-fit for strength compared to rank was linear (Pearson's $R^2 = 0.98$, $p < .0001$). However, at rank position 153, a point of inflection was identified in the rank-order chart. At this position, strength began increasing exponentially. The twenty-seven ROIs with average strength values at or above this point of inflection were considered areas of high strength (HS). These regions are summarized in Table 1 and displayed on a representative subject brain in Fig. 2. While some ROIs associated with high strength were present in the frontal, insular, and parietal lobes, most regions were concentrated in the medial occipital and temporal lobes. Because there was no clear indicator to define regions of low strength in the rank-order chart, a lower limit threshold of 20% of all parcellations (i.e. 36 regions) was used to identify regions with low average strength. These cortical regions are summarized in Table 2. Fig. 3 shows the spatial distribution of these parcellations, which are concentrated predominantly in the lateral occipital lobe.

Because cortical areas with lower strength tended to be smaller by

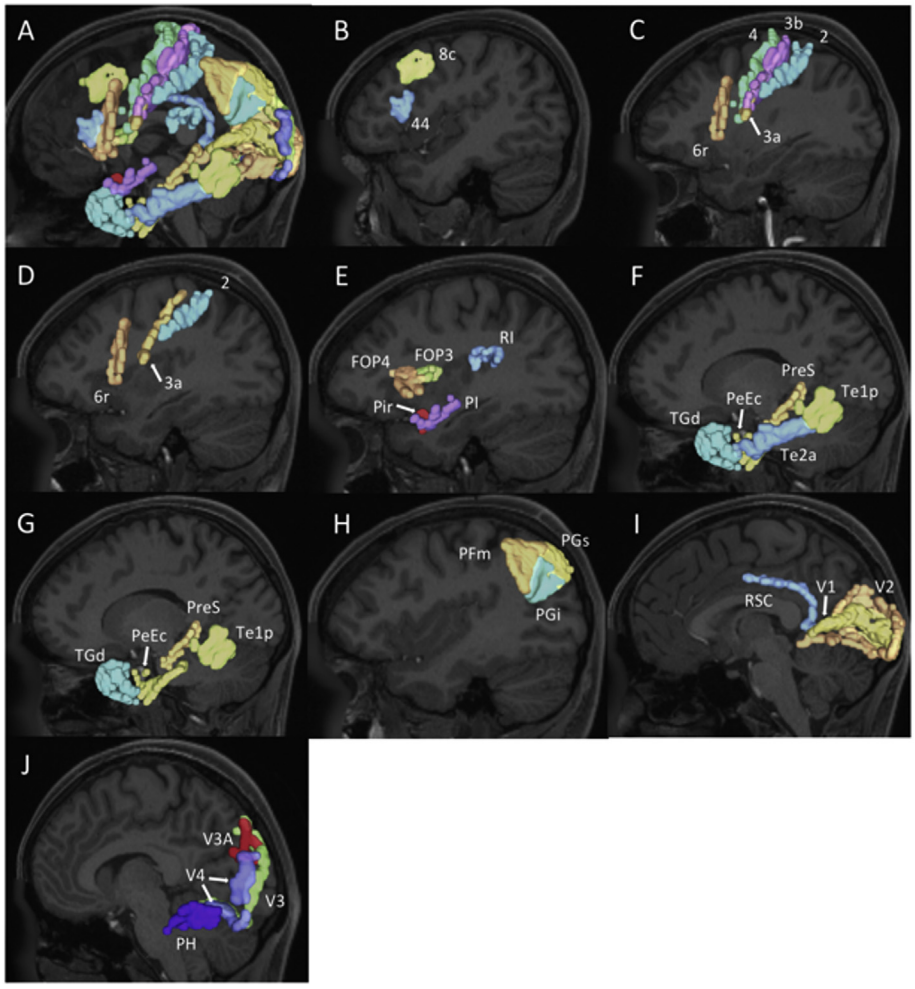

Fig. 2. Cortical distribution of all twenty-seven regions defined as having high average strength. These regions are plotted on sagittal T1-weighted images using a representative subject brain derived from the Human Connectome Project database. (A) All high strength regions are shown unlabeled. (B-J) High strength regions are labeled on sagittal MRI cross-sections and organized into clusters: lateral frontal lobe cluster (B), sensorimotor cluster (C), sensorimotor cluster excluding areas 3b and 4 (D), insula cluster (E), temporal lobe cluster (F), temporal lobe cluster excluding area TE2a (G), inferior parietal lobe cluster (H), medial occipital lobe cluster (I), and a lateral occipital lobe cluster (J).

Table 2
List of cortical regions associated with the lowest average strength.

Cortical region	Average strength ± SEM	Cortical region	Average strength ± SEM
7AL	421 ± 70	PCV	294 ± 92
Ig	418 ± 98	p24	290 ± 80
A1	416 ± 81	7Am	282 ± 57
LBelt	404 ± 89	VMV1	281 ± 57
24dv	401 ± 78	LO1	278 ± 53
10r	400 ± 13	31a	276 ± 37
d23ab	387 ± 88	10v	264 ± 18
VVC	385 ± 12	13I	261 ± 15
TPOJ3	380 ± 10	47 m	241 ± 71
V8	376 ± 75	5 L	238 ± 46
AVI	359 ± 97	LO2	224 ± 59
MT	341 ± 11	PIT	221 ± 61
31pd	330 ± 90	MST	220 ± 50
VIP	326 ± 76	7Pm	175 ± 52
IFJa	314 ± 70	s32	132 ± 48
V4 t	309 ± 66	5 m	126 ± 28
VMV3	297 ± 10	pOFC	125 ± 33
47 s	296 ± 34	25	109 ± 44

volume compared to those with higher strength, we used the Spearman Correlation Test to assess for a correlation between ROI volume and strength (Fig. 4). A significant correlation between volume and strength was identified (Pearson $R = 0.74$, $p < .0001$), even when accounting for outlier regions with volumes three standard deviations above the mean (Pearson $R = 0.61$, $p < .0001$). Given this correlation, we standardized the average strength for each region by its volume. Fig. 5 shows the distribution of standardized strength values based on rank. Similar to the rank-order chart for non-standardized strength values (Fig. 1), the rank-order chart for standardized strength values demonstrated a linear trend to rank 153, followed by an exponential increase in standardized strength with two clear outliers, corresponding to areas 4 and Pir in our atlas. Overall, when comparing standardized and non-standardized ranks, six regions were found to comprise the list of highest strength ROIs, including areas 4, PIR, PI, FOP3, V3A, and 44. To allow for cross comparison, we tabulated the areas with the highest standardized strength in Table 3 and the lowest standardized strength in Table 4 using the previously established cutoffs for non-standardized strength measurements. Table 5 lists the regions that underwent the largest change in rank wen standardizing average strength by volume. Area 3b demonstrated the largest change in rank when accounting for volume, decreasing 148 ranks in total. Similarly, sensorimotor areas 1 and 2 decreased 136 and 128 ranks, respectively.

Coefficients of variation for each ROI were also calculated to assess the variability in the strength measured for each region within our atlas. Tables 6 and 7 summarize the cortical areas with high and low coefficients of variation, respectively, based on a threshold of greater than one standard deviation from mean covariance. While low coefficients of variation were consistently within 1.5 standard deviations from the mean, high coefficients of variation were as large as 5.1 standard deviations from the mean. Areas with high coefficients of variation included PIR, MIP, IFJp, TGV, 13 L, a24pr, and 10v.

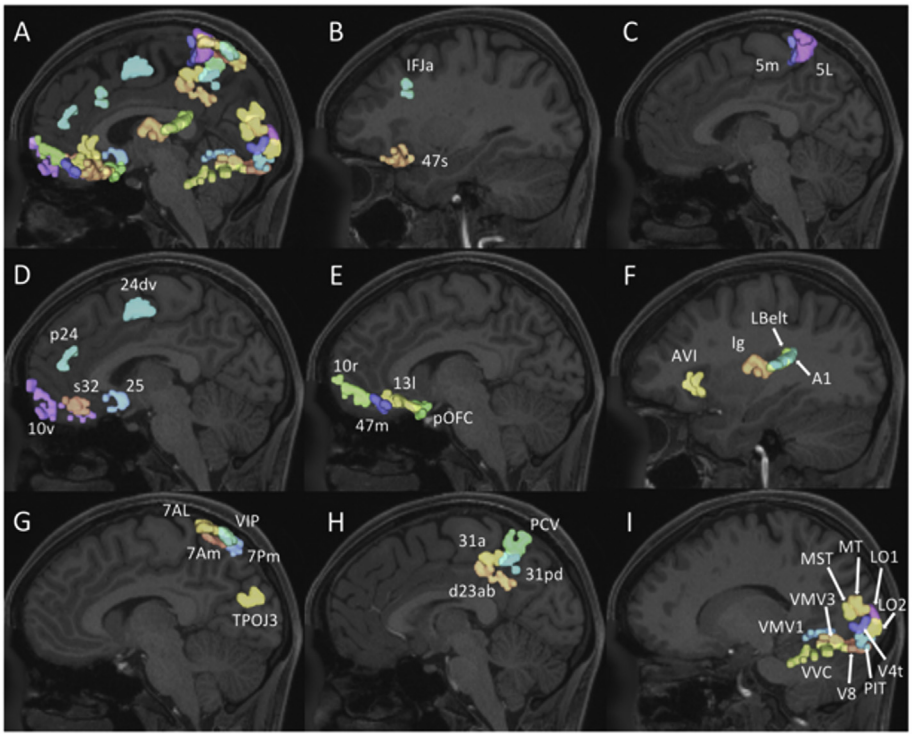

Fig. 3. Cortical distribution of all thirty-six regions defined as having low average strength. These regions are plotted on sagittal T1-weighted images using a representative subject brain derived from the Human Connectome Project database. (A) All low strength regions are shown unlabeled. (B–I) Low strength regions are labeled on sagittal MRI cross-sections and organized into clusters: lateral frontal lobe cluster (B), paracentral lobule cluster (C), medial frontal lobe and cingulate cluster (D), orbitofrontal cluster (E), insula and superior temporal lobe cluster (F), superior parietal lobule cluster (G), precuneus cluster (H), and an occipital lobe cluster (I).

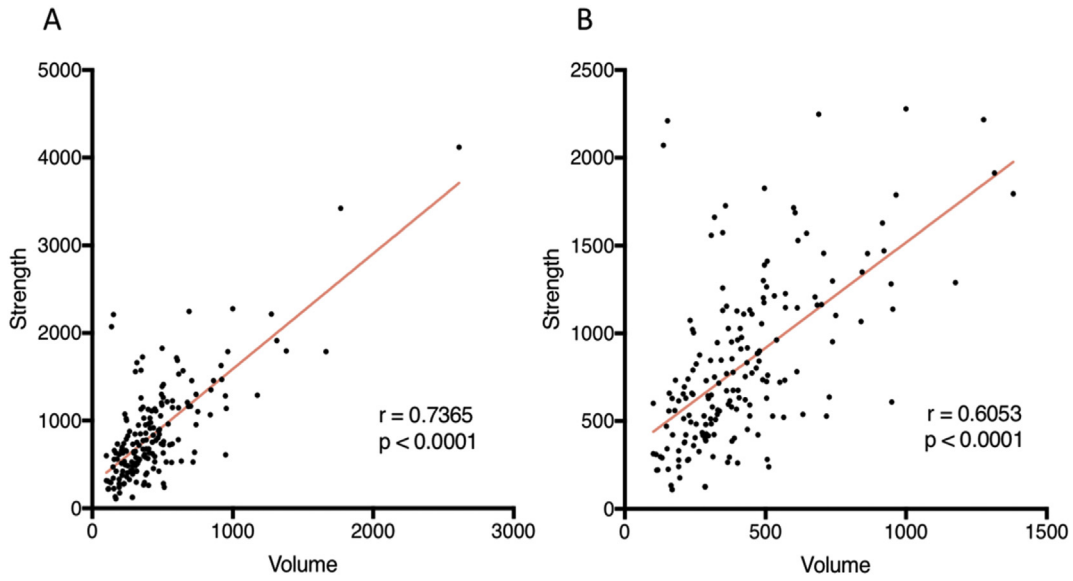

Fig. 4. Correlation between strength and volume. Regions were plotted by strength and volume, (A) with and (B) without outliers (defined as regions with volumes greater than three standard deviations above the mean volume). Spearman's Correlation Test was used to generate a line-of-best-fit for all regions plotted (red lines in both panels). The statistical test revealed a significant positive correlation between the average strength of cortical regions and their volume. (For interpretation of the references to colour in this figure legend, the reader is referred to the web version of this article.)

4. Discussion

In this study, we constructed structural graphs in DSI Studio using imaging data derived from eight individual subjects made available through the HCP. Using these graphs, we were able to quantify the strength between all 180 cortical regions included in our atlas. In reviewing our work related to these regions [15–23], we find that several cortical areas associated with high strength correspond to uniquely eloquent brain regions related to primary sensorimotor function, primary visual processing, and speech production in the left cerebral hemisphere. Other cortical areas are associated with higher-order functional networks like visuospatial processing and attention.

4.1. Strength and cortical eloquence

In reviewing the list of areas associated with high average strength, one important pattern emerged. Several of the areas associated with high strength represent eloquent parts of the human neocortex associated with critical neurologic functions that may be disrupted if the cortex is damaged during surgery. For example, area 4 is located in the primary motor cortex, and is responsible for fine motor control of the distal forearms and fingers [24,25]. Areas 1, 2, and 3b were also found

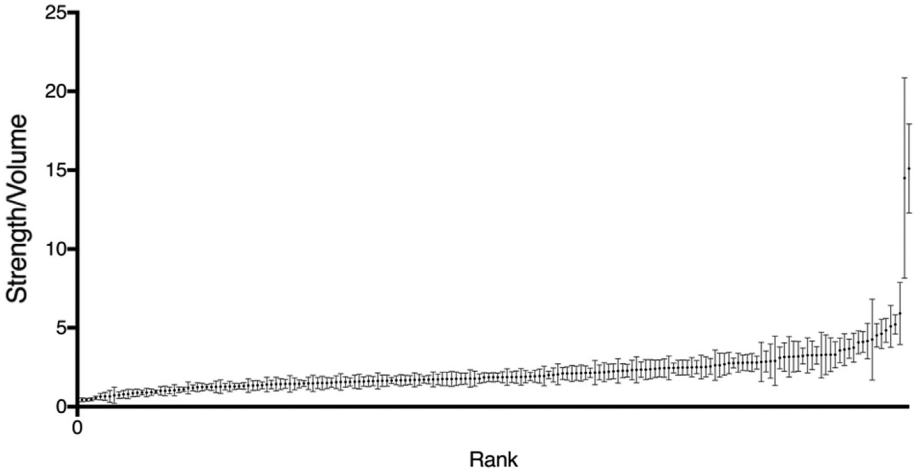

Fig. 5. Ranked distribution of all 180 cortical regions included in our atlas according to their average strength standardized by their volume. Regions are plotted in order of least to greatest strength. Dots signify the mean strength with associated standard error bars.

Table 3
List of cortical regions associated with the highest average strength standardized by ROI volume.

Cortical region	Volume (mm^3)	Average strength	Average strength standardized by volume
4	137.1	2071 ± 386	15.11 ± 2.81
PIR	152.3	2210 ± 969	14.51 ± 6.36
33pr	101.6	600 ± 200	5.91 ± 1.96
PI	318.4	1661 ± 196	5.22 ± 0.61
FOP3	306.6	1559 ± 406	5.08 ± 1.32
V3A	357.4	1727 ± 271	4.83 ± 0.75
STGa	232.4	1074 ± 218	4.62 ± 0.93
44	347.7	1575 ± 259	4.53 ± 0.74
a24pr	240.2	1022 ± 614	4.26 ± 2.55
V7	158.2	658 ± 178	4.16 ± 1.12
TA2	244.1	1003 ± 161	4.11 ± 0.65
V3B	179.7	733 ± 130	4.08 ± 0.72
VMV2	168.0	630 ± 155	3.75 ± 0.92
PreS	496.1	1826 ± 303	3.68 ± 0.61
MBelt	347.7	1259 ± 348	3.62 ± 0.99
s6–8	156.3	558 ± 123	3.57 ± 0.78
IFSp	265.6	877 ± 221	3.30 ± 0.83
i6–8	210.9	695 ± 224	3.29 ± 1.06
PEF	224.6	739 ± 283	3.29 ± 1.25
IFJp	242.2	790 ± 351	3.26 ± 1.44
6r	689.5	2248 ± 382	3.26 ± 0.55
PHA3	347.7	1130 ± 317	3.25 ± 0.91
FOP2	253.9	825 ± 283	3.25 ± 1.11
FOP1	191.4	615 ± 96	3.21 ± 0.50
AAIC	361.3	1155 ± 343	3.20 ± 0.94
LO3	148.4	470 ± 146	3.17 ± 0.98
V3CD	207.0	655 ± 266	3.16 ± 1.28

to have high average strength. These areas localize to the primary sensory cortex and are each involved in critical sensory processes related to touch and proprioception [26–30].

Early visual processing areas, such as V1, V2, V3, and V4 on the medial and polar surfaces of the occipital lobe were also associated with high average strength. These areas are involved in sequential aspects of visual processing [31–35]. Area V1 is considered the primary visual cortex and is particularly involved in motion detection [31,32]. Area V2 is important for foreground-background distinction [33]. Area V3 is involved in perceiving and integrating global motion [31]. Area V4 is involved in the perception of colour as well as images in the peripheral visual field [34,35]. Area V3A, one of the areas of greatest standardized and non-standardized strength, is one area of cortex important in dorsal visual stream processing [36].

Several other areas, including areas 44, FOP3, and FOP4 are important in language. For example, both area 44, which forms part of Broca's complex [37,38], and the fronto-opercular areas (FOP3 and FOP4) are involved in language production [37–42]. FOP3 and FOP4 are also involved in the retrieval of lexical information and in the processes of learning language [41,42]. Additional cortical areas with high strength involved in primary cortical activity include PIR and RI. Area PIR, also called the piriform cortex, is the primary olfactory center and is associated with limbic processes related to emotion and memory [43,44]. Area RI registers primary somatosensory input and integrates this information with auditory signaling [45,46].

4.2. Strength and higher-order cortical functioning

Many cortical areas associated with high strength are involved in complex visual processing. For example, the TE areas, area PGi, and area PE are involved in the higher-order visual processing related to facial recognition [10,47–49]. Areas TE1p and TE2a are also involved in visual working memory [10], while area PGi is involved in detecting changes in visuospatial motion [50]. Area PeEc has roles in semantic identification and integration of an object's spatio-temporal information [47]. Other high strength areas are involved in attention-related processing and understanding visuospatial relationships, such areas PGs, 8C, RSC, PH, and PFm. For example, area PGs plays a role in changes to visuospatial attention in response to biological motion [50]. Area 8C contributes to the maintenance of spatial information as well as the complex visual processing associated with maintaining attention [51,52]. Area RSC, also called the retrosplenial cortex, is primarily responsible for changes in perspective and contributes to spatial navigation [10,53–55]. Area PH is involved in the holistic processing of visual inputs, including the production of spatial maps and location recognition [56,57]. This area is also involved in object recognition [56,57]. Area PFm, in addition to its roles in attention and reorientation, is involved in several higher-order cognitive processes, including syntactical language processing and task-related risk assessment [58,59].

4.3. Strength and volume

Some have warned against broadly applying graph theory to the brain without standardizing for ROI volume [60]. In doing this, we identified a significant correlation between node volume and average strength (Fig. 4). However, we would argue that this correlation better reflects the critical neurologic functions that are associated with areas of high strength. In other words, larger areas of cortex are associated with increasing average strength because the brain requires significant

Table 4
List of cortical regions associated with the lowest average strength standardized by ROI volume.

Cortical region	Volume (mm^3)	Average strength	Average strength standardized by volume
STSdp	550.781	721 ± 124	1.31 ± 0.22
2	1380.86	1794 ± 242	1.29 ± 0.17
8Ad	568.359	733 ± 113	1.29 ± 0.19
9 m	738.281	952 ± 242	1.29 ± 0.32
POS2	611.328	781 ± 125	1.27 ± 0.20
TF	839.844	1067 ± 365	1.27 ± 0.43
47 m	191.406	241 ± 71.	1.25 ± 0.37
OP4	503.906	630 ± 109	1.25 ± 0.21
31a	222.656	276 ± 37.	1.24 ± 0.17
VMV1	226.563	281 ± 57.	1.24 ± 0.25
VIP	263.672	326 ± 76.	1.23 ± 0.29
6a	953.125	1138 ± 179	1.19 ± 0.18
10d	443.359	529 ± 169	1.19 ± 0.38
1	1175.78	1289 ± 164	1.09 ± 0.13
3b	1664.06	1788 ± 304	1.07 ± 0.18
11l	435.547	452 ± 158	1.03 ± 0.36
24dv	388.672	401 ± 78.	1.03 ± 0.20
VVC	380.859	385 ± 122	1.01 ± 0.32
24dd	525.391	527 ± 143	1.00 ± 0.27
47 s	312.5	296 ± 34.	0.94 ± 0.11
5 mv	564.453	522 ± 117	0.92 ± 0.20
7Pm	195.313	175 ± 52.	0.90 ± 0.26
7AL	472.656	421 ± 70.	0.89 ± 0.14
23c	726.563	637 ± 171	0.87 ± 0.23
SCEF	632.813	538 ± 145	0.85 ± 0.22
s32	164.063	132 ± 48.	0.80 ± 0.29
PCV	371.094	294 ± 92.	0.79 ± 0.24

Table 5
Largest changes in node rank FOLLOWING standardization by node volume.

ROI	Rank based on average strength	Rank based on standardized strength	Change in rank
3b	170	22	−148
2	171	35	−136
IFJa	22	152	130
1	151	23	−128
PFm	173	48	−125
V1	180	58	−122
V4 t	21	143	122
6a	137	25	−112
LO3	43	155	112
PF	150	40	−110
33pr	68	178	110
s6–8	60	165	105
VMV3	20	121	101
TGd	176	78	−98
TE2a	159	61	−98
TF	129	31	−98
p24	17	114	97
VMV2	74	168	94
MST	6	100	94

structural connections to these eloquent areas, e.g. for fine motor movement, visual processing, or language production. In addition, it may be more appropriate within the field of neurosurgery to analyze absolute changes in strength across the cortex, for example, when patients undergo resection of glial tumors that have disrupted subcortical white matter pathways, since strength fundamentally represents the total number of nerve fibers connected to a given region.

4.4. Strength variation

It is well known that the human connectome varies considerably from person to person, in both healthy and diseased states [61–63]. Therefore, it was expected that our sample of eight subjects would have some variation. Indeed, the distribution of coefficients of variation suggests that some regions have considerably more variation in average strength compared to others within our atlas. For example, the coefficients of variation for four cortical regions, including areas 13 L, 10 V, a24pr, and TGV, were greater than three standard deviations from the mean (Tables 6, 7). This variation likely reflects two things, (1) our limited sample size and (2) fundamental anatomic differences between the HCP subjects used to construct our structural graphs.

4.5. Strength in neuropsychiatric disease and its application to clinical neurosurgery

Some studies have analyzed the effects of different neuropsychiatric conditions on nodal strength using functional graphs. For example, one group has postulated that increased strength in primary visual areas contributes to improvement in facial recognition skills in adults compared to children [64]. Another study has reported increases in nodal strength between regions related to audition in individuals presenting with sudden sensorineural hearing loss [65]. Other studies have shown that strength within the primary sensorimotor cortex is reduced in patients with Parkinson's Disease [66,67], and others have demonstrated decreased network strength across the bilateral orbital regions of the superior frontal gyri and putamen in children presenting with absence seizures [68].

While these studies focus on functional rather than structural brain graphs [64,65,69], they suggest that strength is a dynamic graphical measure that changes with the developing brain and in the presence of disease. Despite the utilization of intra-operative fiber tractography to preserve white matter tracts during brain surgery, it is not currently routine for neurosurgeons to quantify properties of the connectome or measure them over a patient's clinical course. As demonstrated in this study, though, graph metrics can shed light on important underlying properties within the cortex. With larger clinical data sets, future application of these metrics may be used to understand how intrinsic brain tumors disrupt the connectome and its underlying properties. In this regard, strength may have clinical utility within neurosurgery if (1) the metric can be measured and monitored over time, and (2) changes in the metric can be correlated with changes in neurologic function.

5. Conclusions

Strength is an important graph theory metric that quantifies the number of structural nerve fiber connections to a given region of cortex. We have found that regions of average high strength within the left cerebral hemisphere tend to localize to eloquent areas of the brain, such as the primary sensorimotor cortex, primary visual cortex, and Broca's area. Other areas of high strength are involved in complex higher-order visuospatial and attentional processing. Future studies will examine the dynamic effects of neurologic disease on this metric, including the effects of brain tumor surgery, to better understand how strength correlates with neurologic function.

Supplementary data to this article can be found online at https://doi.org/10.1016/j.jns.2019.116529.

Disclosures

The authors report no conflict of interest concerning the materials or methods used in this study or the findings specified in this paper.

Funding

None.

Declaration of Competing Interest

None.

Table 6
Cortical areas with high coefficients of variation for strength.

ROI	Coefficient of variation	*Z*-Score
10v	200.3	5.13
a24pr	169.9	3.95
13 L	164.6	3.74
TGv	152.9	3.28
IFJp	125.6	2.21
MIP	124.4	2.16
PIR	124.0	2.15
25	115.7	1.82
V3CD	114.6	1.78
PEF	108.2	1.53
PHA1	106.1	1.45
8BM	104.2	1.37
s32	103.6	1.35
23d	102.7	1.31
SFL	100.0	1.21
VMV3	99.5	1.19
11l	98.8	1.16
LIPv	97.3	1.10
FOP2	96.9	1.09
TF	96.7	1.08
MT	96.0	1.05
PHA2	95.9	1.05

Table 7
Cortical areas with low coefficients of variation for strength.

ROI	Coefficient of variation	Z-score
PFcm	31.7	−1.47
8Av	31.8	−1.46
46	32.3	−1.44
47 s	33.3	−1.40
PI	33.4	−1.40
PBelt	35.0	−1.34
PFt	35.7	−1.31
1	36.0	−1.30
9-46d	36.3	−1.29
A5	38.0	−1.22
2	38.3	−1.21
31a	38.8	−1.19
45	39.2	−1.17
PH	40.8	−1.11
POS1	41.9	−1.07
a9-46v	42.1	−1.06

Acknowledgements

None.

References

[1] O. Ajilore, M. Lamar, A. Leow, A. Zhang, S. Yang, A. Kumar, Graph theory analysis of cortical-subcortical networks in late-life depression, Am. J. Geriatr. Psychiatry 22 (2) (2014) 195–206.
[2] A. Dhand, J. Harp, S.P. Borgatti, Leadership in neurology: a social network analysis, Ann. Neurol. 75 (3) (2014) 342–350.
[3] D. Hincapie, J. Ospina, Algebraic analysis of social networks for bio-surveillance: the cases of SARS-Beijing-2003 and AH1N1 influenza-Mexico-2009, Adv. Exp. Med. Biol. 696 (2011) 751–761.
[4] B. Martinez-Lopez, A.M. Perez, J.M. Sanchez-Vizcaino, Social network analysis. Review of general concepts and use in preventive veterinary medicine, Transbound. Emerg. Dis. 56 (4) (2009) 109–120.
[5] F. Vecchio, F. Miraglia, P. Bramanti, P.M. Rossini, Human brain networks in physiological aging: a graph theoretical analysis of cortical connectivity from EEG data, J. Alzheimers Dis. 41 (4) (2014) 1239–1249.
[6] E.T. Bullmore, D.S. Bassett, Brain graphs: graphical models of the human brain connectome, Annu. Rev. Clin. Psychol. 7 (2011) 113–140.
[7] C.E. Hugenschmidt, J.H. Burdette, A.R. Morgan, J.D. Williamson, S.B. Kritchevsky, P.J. Laurienti, Graph theory analysis of functional brain networks and mobility disability in older adults, J. Gerontol. A Biol. Sci. Med. Sci. 69 (11) (2014) 1399–1406.
[8] J. Song, V.A. Nair, W. Gaggl, V. Prabhakaran, Disrupted brain functional organization in epilepsy revealed by graph theory analysis, Brain Connect. 5 (5) (2015) 276–283.
[9] J.A. Brown, J.D. Rudie, A. Bandrowski, J.D. Van Horn, S.Y. Bookheimer, The UCLA multimodal connectivity database: a web-based platform for brain connectivity matrix sharing and analysis, Front Neuroinform 6 (2012) 28.
[10] M.F. Glasser, T.S. Coalson, E.C. Robinson, C.D. Hacker, J. Harwell, E. Yacoub, et al., A multi-modal parcellation of human cerebral cortex, Nature 536 (7615) (2016) 171–178.
[11] F.-C. Yeh, V.J. Wedeen, T. W-YI, Generalized Q-sampling imaging, IEEE Trans. Med. Imaging 29 (9) (2010) 1626–1635.
[12] D.C. Van Essen, M.F. Glasser, The human connectome project: progress and prospects, Cerebrum: The Dana Forum on Brain Science 2016 (2016) cer-10-6.
[13] A.C. Evans, S. Marrett, P. Neelin, L. Collins, K. Worsley, W. Dai, et al., Anatomical mapping of functional activation in stereotactic coordinate space, NeuroImage 1 (1) (1992) 43–53.
[14] J. Martino, P.C.D.W. Hamer, M.S. Berger, M.T. Lawton, C.M. Arnold, E.M. de Lucas, et al., Analysis of the subcomponents and cortical terminations of the perisylvian superior longitudinal fasciculus: a fiber dissection and DTI tractography study, Brain Struct. Funct. 218 (1) (2013) 105–121.
[15] C.M. Baker, J.D. Burks, R.G. Briggs, A.K. Conner, C.A. Glenn, G. Sali, et al., A Connectomic atlas of the human cerebrum-chapter 1: introduction, methods, and significance, Oper. Neurosurg. (Hagerstown) 15 (suppl_1) (2018) S1–s9.
[16] C.M. Baker, J.D. Burks, R.G. Briggs, A.K. Conner, C.A. Glenn, K. Manohar, et al., A Connectomic atlas of the human cerebrum-chapter 8: the posterior cingulate cortex, medial parietal lobe, and parieto-occipital sulcus, Oper. Neurosurg. (Hagerstown) 15 (suppl_1) (2018) S350–s71.
[17] C.M. Baker, J.D. Burks, R.G. Briggs, A.K. Conner, C.A. Glenn, J.P. Morgan, et al., A connectomic atlas of the human cerebrum-chapter 2: the lateral frontal lobe, Oper. Neurosurg. (Hagerstown) 15 (suppl_1) (2018) S10–s74.
[18] C.M. Baker, J.D. Burks, R.G. Briggs, A.K. Conner, C.A. Glenn, J.M. Robbins, et al., A connectomic atlas of the human cerebrum-chapter 5: the insula and opercular cortex, Oper. Neurosurg. (Hagerstown) 15 (suppl_1) (2018) S175–s244.
[19] C.M. Baker, J.D. Burks, R.G. Briggs, A.K. Conner, C.A. Glenn, K.N. Taylor, et al., A Connectomic atlas of the human cerebrum-chapter 7: the lateral parietal lobe, Oper. Neurosurg. (Hagerstown) 15 (suppl_1) (2018) S295–s349.
[20] C.M. Baker, J.D. Burks, R.G. Briggs, C.K. Milton, A.K. Conner, C.A. Glenn, et al., A connectomic atlas of the human cerebrum-chapter 6: the temporal lobe, Oper. Neurosurg. (Hagerstown) 15 (suppl_1) (2018) S245–s94.
[21] C.M. Baker, J.D. Burks, R.G. Briggs, J.R. Sheets, A.K. Conner, C.A. Glenn, et al., A connectomic atlas of the human cerebrum-chapter 3: the motor, premotor, and sensory cortices, Oper. Neurosurg. (Hagerstown) 15 (suppl_1) (2018) S75–s121.
[22] C.M. Baker, J.D. Burks, R.G. Briggs, J. Stafford, A.K. Conner, C.A. Glenn, et al., A connectomic atlas of the human cerebrum-chapter 4: the medial frontal lobe, anterior cingulate gyrus, and orbitofrontal cortex, Oper. Neurosurg. (Hagerstown) 15 (suppl_1) (2018) S122–s74.
[23] C.M. Baker, J.D. Burks, R.G. Briggs, J. Stafford, A.K. Conner, C.A. Glenn, et al., A connectomic atlas of the human cerebrum-chapter 9: the occipital lobe, Oper. Neurosurg. (Hagerstown) 15 (suppl_1) (2018) S372–s406.
[24] P.A. Chouinard, T. Paus, The primary motor and premotor areas of the human cerebral cortex, Neuroscientist 12 (2) (2006) 143–152.
[25] M. Coco, V. Perciavalle, P. Cavallari, V. Perciavalle, Effects of an exhaustive exercise on motor skill learning and on the excitability of primary motor cortex and supplementary motor area, Medicine (Baltimore) 95 (11) (2016) e2978.
[26] M. Ploner, F. Schmitz, H.J. Freund, A. Schnitzler, Differential organization of touch and pain in human primary somatosensory cortex, J. Neurophysiol. 83 (3) (2000) 1770–1776.
[27] J. Hyvarinen, A. Poranen, Receptive field integration and submodality convergence in the hand area of the post-central gyrus of the alert monkey, J. Physiol. 283 (1978) 539–556.
[28] R. Martuzzi, W. van der Zwaag, S. Dieguez, A. Serino, R. Gruetter, O. Blanke, Distinct contributions of Brodmann areas 1 and 2 to body ownership, Soc. Cogn. Affect. Neurosci. 10 (11) (2015) 1449–1459.
[29] C.J. Vierck, B.L. Whitsel, O.V. Favorov, A.W. Brown, M. Tommerdahl, Role of primary somatosensory cortex in the coding of pain, Pain 154 (3) (2013) 334–344.
[30] K.J. Huffman, L. Krubitzer, Area 3a: topographic organization and cortical connections in marmoset monkeys, Cereb. Cortex 11 (9) (2001) 849–867.
[31] M. Furlan, A.T. Smith, Global motion processing in human visual cortical areas V2 and V3, J. Neurosci. 36 (27) (2016) 7314–7324.
[32] B.A. Wandell, S.O. Dumoulin, A.A. Brewer, Visual field maps in human cortex, Neuron 56 (2) (2007) 366–383.
[33] F.T. Qiu, R. von der Heydt, Figure and ground in the visual cortex: v2 combines stereoscopic cues with gestalt rules, Neuron 47 (1) (2005) 155–166.
[34] J. Winawer, N. Witthoft, Human V4 and ventral occipital retinotopic maps, Vis. Neurosci. 32 (2015) E020.
[35] J. Larsson, D.J. Heeger, Two retinotopic visual areas in human lateral occipital cortex, J. Neurosci. 26 (51) (2006) 13128–13142.
[36] R.O. Abdollahi, H. Kolster, M.F. Glasser, E.C. Robinson, T.S. Coalson, D. Dierker, et al., Correspondences between retinotopic areas and myelin maps in human visual cortex, NeuroImage 99 (2014) 509–524.
[37] A. Ardila, B. Bernal, M. Rosselli, How localized are language brain areas? A review of brodmann areas involvement in oral language, Arch. Clin. Neuropsychol. 31 (1) (2016) 112–122.
[38] H.T. van Schie, I. Toni, H. Bekkering, Comparable mechanisms for action and language: neural systems behind intentions, goals, and means, Cortex 42 (4) (2006) 495–498.
[39] B. Fischl, N. Rajendran, E. Busa, J. Augustinack, O. Hinds, B.T. Yeo, et al., Cortical folding patterns and predicting cytoarchitecture, Cereb. Cortex 18 (8) (2008)

1973–1980.
[40] J.D. Rolston, D.J. Englot, A. Benet, J. Li, S. Cha, M.S. Berger, Frontal operculum gliomas: language outcome following resection, J. Neurosurg. 122 (4) (2015) 725–734.
[41] Y. Li, H. Yao, P. Lin, L. Zheng, C. Li, B. Zhou, et al., Frequency-dependent altered functional connections of default mode network in Alzheimer's disease, Front. Aging Neurosci. 9 (2017) 259.
[42] H. Steinmetz, R.J. Seitz, Functional anatomy of language processing: neuroimaging and the problem of individual variability, Neuropsychologia 29 (12) (1991) 1149–1161.
[43] D.M. Johnson, K.R. Illig, M. Behan, L.B. Haberly, New features of connectivity in piriform cortex visualized by intracellular injection of pyramidal cells suggest that "primary" olfactory cortex functions like "association" cortex in other sensory systems, J. Neurosci. 20 (18) (2000) 6974–6982.
[44] D.N. Vaughan, G.D. Jackson, The piriform cortex and human focal epilepsy, Front. Neurol. 5 (2014) 259.
[45] E.H. Chudler, R.L. Nahin, D.R. Kenshalo Jr., Distribution and size of GABAergic neurons in area 7b and the retroinsular cortex of the monkey, Brain Res. 481 (2) (1989) 383–387.
[46] T.A. Hackett, Anatomic organization of the auditory cortex, Handb. Clin. Neurol. 129 (2015) 27–53.
[47] Y. Naya, Declarative association in the perirhinal cortex, Neurosci. Res. 113 (2016) 12–18.
[48] R. Rajimehr, J.C. Young, R.B. Tootell, An anterior temporal face patch in human cortex, predicted by macaque maps, Proc. Natl. Acad. Sci. U. S. A. 106 (6) (2009) 1995–2000.
[49] D.Y. Tsao, S. Moeller, W.A. Freiwald, Comparing face patch systems in macaques and humans, Proc. Natl. Acad. Sci. U. S. A. 105 (49) (2008) 19514–19519.
[50] R.B. Mars, S. Jbabdi, J. Sallet, J.X. O'Reilly, P.L. Croxson, E. Olivier, et al., Diffusion-weighted imaging tractography-based parcellation of the human parietal cortex and comparison with human and macaque resting-state functional connectivity, J. Neurosci. 31 (11) (2011) 4087–4100.
[51] M. Petrides, D.N. Pandya, Dorsolateral prefrontal cortex: comparative cytoarchitectonic analysis in the human and the macaque brain and corticocortical connection patterns, Eur. J. Neurosci. 11 (3) (1999) 1011–1036.
[52] D.H. Reser, K.J. Burman, H.H. Yu, T.A. Chaplin, K.E. Richardson, K.H. Worthy, et al., Contrasting patterns of cortical input to architectural subdivisions of the area 8 complex: a retrograde tracing study in marmoset monkeys, Cereb. Cortex 23 (8) (2013) 1901–1922.
[53] J.P. Aggleton, R.C. Saunders, N.F. Wright, S.D. Vann, The origin of projections from the posterior cingulate and retrosplenial cortices to the anterior, medial dorsal and laterodorsal thalamic nuclei of macaque monkeys, Eur. J. Neurosci. 39 (1) (2014) 107–123.
[54] S.D. Vann, J.P. Aggleton, E.A. Maguire, What does the retrosplenial cortex do? Nat. Rev. Neurosci. 10 (11) (2009) 792–802.
[55] R. Leech, D.J. Sharp, The role of the posterior cingulate cortex in cognition and disease, Brain 137 (1) (2014) 12–32.
[56] K. Grill-Spector, R. Malach, The human visual cortex, Annu. Rev. Neurosci. 27 (2004) 649–677.
[57] R.A. Epstein, Parahippocampal and retrosplenial contributions to human spatial navigation, Trends Cogn. Sci. 12 (10) (2008) 388–396.
[58] S. Caspers, S.B. Eickhoff, T. Rick, A. von Kapri, T. Kuhlen, R. Huang, et al., Probabilistic fibre tract analysis of cytoarchitectonically defined human inferior parietal lobule areas reveals similarities to macaques, NeuroImage 58 (2) (2011) 362–380.
[59] D.B. Shalom, D. Poeppel, Functional anatomic models of language: assembling the pieces, Neuroscientist 14 (1) (2008) 119–127.
[60] M.C. Ottet, M. Schaer, M. Debbane, L. Cammoun, J.P. Thiran, S. Eliez, Graph theory reveals dysconnected hubs in 22q11DS and altered nodal efficiency in patients with hallucinations, Front. Hum. Neurosci. 7 (2013) 402.
[61] A.W. Toga, K.A. Clark, P.M. Thompson, D.W. Shattuck, J.D. Van Horn, Mapping the human connectome, Neurosurgery 71 (1) (2012) 1–5.
[62] C.G. Yan, B. Cheung, C. Kelly, S. Colcombe, R.C. Craddock, A. Di Martino, et al., A comprehensive assessment of regional variation in the impact of head micromovements on functional connectomics, NeuroImage 76 (2013) 183–201.
[63] C.G. Yan, R.C. Craddock, X.N. Zuo, Y.F. Zang, M.P. Milham, Standardizing the intrinsic brain: towards robust measurement of inter-individual variation in 1000 functional connectomes, NeuroImage 80 (2013) 246–262.
[64] J.E. Joseph, J.E. Swearingen, J.D. Clark, C.E. Benca, H.R. Collins, C.R. Corbly, et al., The changing landscape of functional brain networks for face processing in typical development, NeuroImage 63 (3) (2012) 1223–1236.
[65] H. Xu, W. Fan, X. Zhao, J. Li, W. Zhang, P. Lei, et al., Disrupted functional brain connectome in unilateral sudden sensorineural hearing loss, Hear. Res. 335 (2016) 138–148.
[66] A. Nagano-Saito, K. Martinu, O. Monchi, Function of basal ganglia in bridging cognitive and motor modules to perform an action, Front. Neurosci. 8 (2014) 187.
[67] C.Y. Luo, X.Y. Guo, W. Song, Q. Chen, B. Cao, J. Yang, et al., Functional connectome assessed using graph theory in drug-naive Parkinson's disease, J. Neurol. 262 (6) (2015) 1557–1567.
[68] K. Xue, C. Luo, D. Zhang, T. Yang, J. Li, D. Gong, et al., Diffusion tensor tractography reveals disrupted structural connectivity in childhood absence epilepsy, Epilepsy Res. 108 (1) (2014) 125–138.
[69] V. Prckovska, W. Huijbers, A. Schultz, L. Ortiz-Teran, C. Pena-Gomez, P. Villoslada, et al., Epicenters of dynamic connectivity in the adaptation of the ventral visual system, Hum. Brain Mapp. 38 (4) (2017) 1965–1976.